Diet-induced loss of adipose Hexokinase 2 triggers hyperglycemia

Mitsugu Shimobayashi[1*], Sunil Shetty[1†], Irina C. Frei[1†], Bettina K. Wölnerhanssen[2,3], Diana Weissenberger[1], Nikolaus Dietz[1], Amandine Thomas[1], Danilo Ritz[1], Anne Christin Meyer-Gerspach[2,3], Timm Maier[1], Nissim Hay[4], Ralph Peterli[5], Nicolas Rohner[6,7], Michael N. Hall[1*]

[1] Biozentrum, University of Basel, Basel 4056, Switzerland.

[2] St. Clara Research Ltd, St. Claraspital, Basel 4016, Switzerland.

[3] University of Basel, Basel 4056, Switzerland.

[4] Department of Biochemistry and Molecular Genetics, College of Medicine, University of Illinois at Chicago, Chicago, IL 60607, USA.

[5] Clarunis, Department of Visceral Surgery, University Centre for Gastrointestinal and Liver Diseases, Basel 4016, Switzerland.

[6] Stowers Institute for Medical Research, Kansas City, Missouri 64110, USA.

[7] Department of Molecular and Integrative Physiology, KU Medical Center, Kansas City, Kansas 66160, USA

[†] These authors contributed equally to this work.

[*] Corresponding authors:

Klingelbergstrasse 70, Basel 4056, Switzerland

TEL: +41 61 207 2171 (MS)

+41 61 207 2150 (MNH)

e-mail: mitsugu.shimobayashi@unibas.ch (MS)

m.hall@unibas.ch (MNH)

Summary

Chronically high blood glucose (hyperglycemia) leads to type 2 diabetes, fatty liver disease, and cardiovascular disease[1]. Obesity is a major risk factor for hyperglycemia, but the underlying mechanism is unknown. Here we show that a high fat diet (HFD) in mice causes early loss of expression of the glycolytic enzyme Hexokinase 2 (HK2) specifically in adipose tissue. Adipose-specific knockout of *Hk2* caused enhanced gluconeogenesis and lipogenesis in liver, a condition known as selective insulin resistance[2], leading to glucose intolerance. Furthermore, we observed reduced hexokinase activity in adipose tissue of obese patients, and identified a loss-of-function mutation in the *hk2* gene of naturally hyperglycemic Mexican cavefish. Mechanistically, HFD in mice led to loss of HK2 by inhibiting elongation of *Hk2* mRNA translation. Our findings identify adipose HK2 as a critical mediator of systemic glucose homeostasis, and suggest that obesity-induced loss of adipose HK2 is an evolutionarily conserved, non-cell-autonomous mechanism for hyperglycemia.

47 **Main text**

48 Vertebrates mediate glucose homeostasis by regulating glucose production and uptake in
49 specific organs[3]. High blood glucose stimulates pancreatic beta cells to secrete the
50 hormone insulin which in turn promotes glucose uptake in skeletal muscle and adipose
51 tissue and inhibits glucose production in liver. Obesity is highly associated with insulin
52 insensitivity in these peripheral tissues, leading to hyperglycemia. Although the contribution
53 of adipose tissue to glucose clearance is minor[4,5], glucose metabolism in adipocytes is key
54 for systemic glucose homeostasis[6,7]. Insulin activates the protein kinases mammalian target
55 of rapamycin complex 2 (mTORC2) and AKT in adipose tissue to promote glucose uptake[8,9].
56 Furthermore, adipose-specific knockout of these insulin signaling components results in
57 local and systemic insulin insensitivity[10-13], highlighting the physiological importance of the
58 adipose insulin-mTORC2-AKT signaling pathway in glucose homeostasis. However, we and
59 others recently reported that diet-induced obesity in mice causes hyperglycemia despite
60 normal insulin signaling in adipose tissue[14,15]. These observations raise the question, how
61 does obesity cause insulin insensitivity and hyperglycemia without affecting the insulin
62 signaling pathway?

63

64 **HK2 is down-regulated in obese mice and humans**

65 To determine the molecular basis of diet-induced insulin insensitivity in adipocytes and
66 hyperglycemia in mice, we performed an unbiased proteomic analysis on visceral white
67 adipose tissue (vWAT) isolated from C57BL/6JRj wild-type mice fed an HFD or normal diet
68 (ND) for 4 weeks (**Extended Data Fig. 1a-1c**). We detected and quantified 6294 proteins of
69 which 52 and 67 were up- and down-regulated, respectively, in vWAT of HFD-fed mice
70 (**Extended Data Table 1**). The glycolytic enzyme Hexokinase 2 (HK2), expressed in
71 adipose tissue and muscle, was among the proteins significantly down-regulated in vWAT
72 (**Fig. 1a**). HK2 phosphorylates glucose to generate glucose-6-phosphate (G6P), the rate-
73 limiting step in glycolysis, in an insulin-stimulated manner. HK2 caught our attention due to
74 efflux of non-phosphorylated glucose and thus a link of HK2 loss to hyperglycemia. HK2 is
75 the most abundant (~80%) of the three hexokinase isoforms expressed in vWAT but the only
76 one down-regulated upon HFD (**Fig. 1a**). Consistent with a previous study[13], expression of
77 the glucose transporter GLUT4 was not affected in vWAT of 4-week HFD mice. Loss of HK2
78 was confirmed in vWAT and demonstrated in subcutaneous WAT (sWAT) and brown
79 adipose tissue (BAT) of 4-week HFD mice by immunoblotting (**Fig. 1b**). HK2 expression
80 was unchanged in skeletal muscle (**Fig. 1b**), suggesting that an HFD decreases HK2
81 expression specifically in adipose tissue. Consistent with reduced HK2 expression,
82 hexokinase activity was decreased in vWAT and sWAT (**Extended Data Fig. 2)**. A
83 longitudinal study of HFD-fed mice revealed that HK2 down-regulation in sWAT and vWAT

occurred already at one week of HFD and correlated with hyperglycemia (**Extended Data Fig. 3a-3e**). GLUT4 was down-regulated only in sWAT and only after ≥2 weeks of HFD. Confirming earlier observations[14,15], insulin signaling was normal at 4 weeks of HFD. Shifting the diet from HFD to ND for 2 weeks restored HK2 expression and normal blood glucose levels (**Fig. 1c** and **Extended Data Fig. 3d**), suggesting that loss of HK2 upon HFD is a transient physiological response. Furthermore, the finding that HK2 expression inversely correlated with hyperglycemia suggests that loss of adipose HK2 may be causal for loss of glucose homeostasis. Omental WAT (human vWAT) biopsies from obese non-diabetic and obese diabetic patients displayed reduced HK activity which inversely correlated with body mass index (BMI) (**Fig. 1d and 1e** and **Extended Data Table 2**), consistent with the previous observation that HK2 expression is decreased in adipose tissue of diabetic patients[16]. These findings suggest that HK2 down-regulation is a key event, possibly causal, in obesity-induced insulin insensitivity and hyperglycemia in mouse and human.

A loss-of-function mutation in cavefish *hk2*

Mexican cavefish (*Astyanax mexicanus*), also known as blind fish, are hyperglycemic compared to surface fish from which they are descended[17](**Fig. 1f** and **1g**). Insulin resistance and hyperglycemia, although a pathological condition in mouse and human, is a selected trait that allows cave-dwelling fish to survive in nutrient-limited conditions. Among three independently evolved cavefish isolates, Pachón and Tinaja cavefish (names refer to the caves from which the fish were isolated) contain a loss-of-function mutation in the insulin receptor, causing insulin resistance and hyperglycemia[17] (**Fig. 1g**). The third isolate, Molino cavefish, is the most hyperglycemic but contains a wild-type insulin receptor and displays normal insulin signaling[17]. Since the phenotype of the Molino fish is similar to that of HFD-fed mice, we hypothesized that this cavefish may be hyperglycemic due to a loss-of-function mutation in the *hk2* gene. DNA sequencing of the *hk2* gene of surface fish and the three cavefish variants revealed a mutation in the *hk2* gene uniquely in Molino. The homozygous, missense mutation in the coding region of the Molino *hk2* gene changed highly conserved arginine 42 (R42) to histidine (R42H) (**Fig. 1h** and **Extended Data Fig. 4b**). Based on the published structure of HK2 [18], R42 forms a salt bridge with aspartic acid 272 (D272) to stabilize the conformation of HK2 (**Extended Data Fig. 4b**), predicting that R42H destabilizes HK2 and is thus a loss-of-function mutation. To test this prediction, we over-expressed wild-type HK2 (HK-WT) and HK2 harboring the Molino mutation (HK2-R42H) in HEK293T cells which have low intrinsic hexokinase activity. HK2-R42H displayed ~50% lower hexokinase activity compared to HK2-WT, despite similar expression levels, suggesting that R42H is indeed a loss-of-function mutation (**Fig. 1i** and **Extended Data Fig.**

121 **4c**). To test further whether the HK2-R42H allele is loss-of-function, we generated a knock-
122 in mouse in which the Molino missense mutation (R42H) is introduced into the mouse *Hk2*
123 gene by CRISPR-Cas9 gene editing (**Extended Data Fig 5a** and **5b**). Upon crossing
124 heterozygous $Hk2^{R42H/+}$ mice, we obtained offspring at the non-mendelian ratio of 18:91:49
125 (R42H homozygous:R42H heterozygous:wild-type) (**Extended Data Table 3**). We note that
126 our $Hk2^{R42H}$ allele is a full body knock-in and that a full body homozygous *Hk2* knockout is
127 embryonic lethal[19]. Together, the above findings in cells and mice suggest that R42H is a
128 partial loss-of-function mutation and may account for the hyperglycemia in Molino cavefish.
129 In other words, it appears that R42H in Molino is a genetically fixed version of what we
130 observe in mice as a physiological down-regulation of HK2 in response to HFD. The
131 findings in Molino provide orthogonal evidence that the down-regulation of HK2 in mice is
132 physiologically relevant. Further experiments with R42H mice were inconclusive due to
133 small littermate cohorts and high variation, although in some cases hyperglycemia was
134 observed.
135
136 **Adipose-specific *Hk2* knockout causes hyperglycemia**
137 The above findings altogether suggest that adipose-specific loss of HK2 may be a cause of
138 insulin insensitivity and hyperglycemia. To test this hypothesis, we first generated a stable
139 HK2 knockdown pre-adipocyte 3T3-L1 cell line (**Extended Data Fig. S6a** and **S6b**). HK2
140 knockdown pre-adipocytes differentiated normally to produce mature adipocytes (**Extended**
141 **Data Fig. 6c** and **6d**). The glycolytic rate was lower in HK2 knockdown adipocytes
142 compared to controls, as measured by extracellular acidification rate (ECAR) (**Fig. 2a**) and
143 lactate production (**Fig. 2b**). Furthermore, although basal glucose uptake did not differ,
144 insulin-stimulated glucose uptake was 50% lower in HK2 knockdown adipocytes (**Fig. 2c**).
145 Thus, loss of HK2 causes insulin insensitivity in adipocytes *in vitro*.
146 To examine further the role of adipose HK2 in glucose homeostasis, and in particular
147 the causality of HK2 loss in hyperglycemia, we generated an adipose-specific *Hk2* knockout
148 (AdHk2KO) mouse. In AdHk2KO mice, HK2 expression was decreased in vWAT, sWAT,
149 and BAT but unchanged in skeletal muscle (**Fig. 2d, Extended Data Fig. 7a** and **7b**), similar
150 to HFD-fed mice (**Fig. 1b**). AdHk2KO mice displayed slightly less fat mass and slightly more
151 lean mass than controls, but no difference in overall body weight (**Extended Data Fig. 7c**
152 and **7d**). No significant difference was observed in organ weight, except for a small
153 decrease in vWAT and a small increase in liver weight (**Extended Data Fig. 7e** and **7f).**
154 Importantly, AdHk2KO mice were insulin insensitive and severely glucose intolerant (**Fig. 2e**
155 and **2f**). These findings suggest that loss of HK2 specifically in adipose tissue causes
156 insulin insensitivity and hyperglycemia.
157

158 **Regulation of liver metabolism by adipose HK2**

159 Adipose tissue accounts for ≤5% of glucose disposal[4,5]. Thus, the severe glucose
160 intolerance observed in AdHk2KO mice (**Fig. 2f**) cannot be explained solely by impaired
161 glucose uptake into adipose tissue. One possible explanation for the severity of the glucose
162 intolerance could be impaired insulin secretion. However, plasma insulin levels were similar
163 in AdHk2KO and control mice (**Extended Data Fig. 7g**). Moreover, insulin signaling (AKT-
164 pS473) was not affected in adipose tissue, skeletal muscle, and liver of AdHk2KO mice (**Fig.
165 2d** and **Extended Data Fig. 7b**), suggesting that hyperglycemia in AdHk2KO mice is not
166 due to a defect in insulin signaling in peripheral tissues.

167 Another potential explanation for the severity of glucose intolerance in AdHk2KO
168 mice is derepressed hepatic glucose production. Adipose tissue is known to impinge
169 negatively on glucose production in liver [6,11,13,20], the main glucose producing organ. To
170 examine whether AdHk2KO mice display enhanced hepatic glucose production, we first
171 performed a pyruvate tolerance test (PTT). AdHk2KO mice displayed significantly higher
172 glucose production compared to controls (**Fig. 3a**). We next examined expression of
173 gluconeogenic genes (*G6pc* and *Pepck*) in liver. Consistent with the observed increase in
174 glucose production, gluconeogenic genes were upregulated in AdHk2KO liver (**Fig. 3b**).
175 These findings suggest that enhanced hepatic gluconeogenesis accounts for the severity of
176 glucose intolerance in AdHk2KO mice. Thus, loss of adipose HK2 non-cell-autonomously
177 promotes hepatic gluconeogenesis and thereby hyperglycemia.

178 We observed enhanced hepatic gluconeogenesis in AdHk2KO mice despite normal
179 systemic insulin signaling, including in liver. To investigate this apparent contradiction, we
180 examined lipogenic gene expression, another readout for hepatic insulin action. Sterol
181 regulatory element-binding protein 1c (SREBP1c) is a transcription factor that activates
182 lipogenic genes and thereby promotes *de novo* lipogenesis in the liver[21]. Expression of
183 SREBP1c and its target fatty acid synthesis genes (*Acly*, *Scd1*, *Fasn*, and *Acc*) were
184 increased in liver of AdHk2KO mice (**Fig. 3c**), suggesting that loss of adipose HK2 also
185 promotes hepatic lipogenesis. The increased hepatic gluconeogenesis and lipogenesis in
186 AdHk2KO mice mimics a condition in diabetic patients known as selective insulin resistance[2]
187 (see below). Thus, loss of adipose HK2 may cause selective insulin resistance and thereby
188 contribute to the pathogenesis of type 2 diabetes.

189 We note that hepatic triglyceride (TG) levels were unchanged in AdHk2KO mice
190 despite increased expression of lipogenic genes (**Extended Data Fig. 7h**). Most likely, *de*
191 *novo*-synthesized TG in AdHk2KO liver is delivered to adipose tissue for storage. This is
192 consistent with our observations that adipose tissue mass is largely unaffected in AdHk2KO
193 mice.
194

195 **HK2 activates ChREBP in adipose tissue**

196 How does adipose HK2 control hepatic gluconeogenesis? As shown previously, adipose-
197 specific knockout of carbohydrate-responsive element binding protein (ChREBP) decreases
198 adipose lipogenesis and increases hepatic gluconeogenesis[20,22]. Furthermore, HFD inhibits
199 adipose ChREBP and lipogenesis via an unknown mechanism proposed to involve glucose
200 or a glucose metabolite[23]. G6P, a glucose metabolite and product of HK2, promotes
201 ChREBP activity in a rat insulinoma cell line[24]. Thus, we hypothesized that HFD-induced
202 loss of HK2 and a concomitant decrease in G6P leads to loss of both ChREBP activity and
203 lipogenesis in adipose tissue. To test this hypothesis, we examined *Chrebp* expression in
204 adipose tissue of AdHk2KO and control mice. ChREBP has two isoforms. Constitutively
205 expressed ChREBPα promotes transcription of ChREBPβ which is then dominant for
206 activation of fatty acid synthesis genes[23]. Expression of *Chrebpβ,* but not *Chrebpα*, was
207 significantly decreased in vWAT, sWAT, and BAT of AdHk2KO mice (**Fig. 3d-3e** and
208 **Extended Data Fig. 7i**). Consistent with reduced *Chrebpβ* expression, fatty acid synthesis
209 genes were down-regulated in vWAT, sWAT, and BAT of AdHk2KO mice (**Fig. 3d-3e** and
210 **Extended Data Fig. 7i**). Thus, HK2 promotes ChREBP activity and lipogenesis in adipose
211 tissue, possibly via G6P. Combined with previous observations[20], our findings suggest that
212 HK2 controls hepatic gluconeogenesis via adipose ChREBP (see below).
213

214 **Mechanism of HFD-induced HK2 down-regulation**

215 Our findings suggest that HFD causes loss of adipose HK2 and thereby triggers
216 hyperglycemia. How does HFD down-regulate adipose HK2? To answer this question, we
217 first examined *Hk2* mRNA expression in HFD- and ND-fed mice. HFD-fed mice exhibited
218 decreased *Hk2* mRNA in sWAT but not in vWAT and BAT (**Fig. 4a**). This suggests that HK2
219 synthesis is down-regulated at the transcriptional level in sWAT, and at a post-transcriptional
220 level in vWAT and BAT. To investigate the post-transcriptional mechanism, we performed
221 polysome profiling on vWAT from HFD- and ND-fed mice. In the presence of cycloheximide
222 to maintain ribosome-mRNA complexes, vWAT lysates from HFD-fed mice contained more
223 polysomes and fewer monosomes (80S ribosome) relative to ND-fed mice (**Fig. 4b**). An
224 increase in polysomes can be due to increased translation initiation or decreased elongation.
225 To distinguish these two possibilities, we performed polysome profiling in the absence of
226 cycloheximide, a condition which allows actively translating ribosomes to run off mRNA.
227 Although there were fewer overall polysomes in the absence cycloheximide, we consistently
228 observed more polysomes in vWAT from HFD-fed mice (**Fig. 4c**), suggesting that HFD
229 inhibits or slows translation elongation of a subset of mRNAs. Shifting the diet from HFD to
230 ND for 2 weeks restored elongation (**Fig. 4d**), as described above for glycemia (**Extended**

231 **Data Fig. 3d**). To determine whether HFD affects elongation of *Hk2* mRNA translation, we
232 measured *Hk2* mRNA in monosome, light polysome, and heavy polysome fractions. *Hk2*
233 mRNA from HFD vWAT was enriched in heavy polysomes, whereas it was enriched in light
234 polysomes in ND vWAT (**Fig. 4e** and **Extended Data Fig. 8a**). Thus, HFD down-regulates
235 HK2 in vWAT by inhibiting elongation of *Hk2* mRNA translation.
236 It was recently reported that the forkhead transcription factors FOXK1 and FOXK2
237 promote *Hk2* transcription in adipose tissue[25]. We investigated whether the transcriptional
238 down-regulation of *Hk2* mRNA in sWAT could be due to loss of FOXK1 and FOXK2. *Foxk1*
239 and *Foxk2* expression was significantly decreased in sWAT, but not in vWAT or BAT, of
240 HFD-fed mice (**Fig. 4f, Extended Data Fig. 8b** and **8c**). Thus, HFD appears to down-
241 regulate HK2 in sWAT by inhibiting FOXK1/2 and, thereby, expression of the *Hk2* gene.
242
243 **Discussion**
244 How obesity causes hyperglycemia is a long-standing question. In this study, we show that
245 a high fat diet causes hyperglycemia by inducing loss of HK2 specifically in adipose tissue.
246 Loss of adipose HK2 leads to hyperglycemia in two ways (**Fig. 4g**). First, HK2 loss results in
247 reduced glucose uptake by adipose tissue due to the inability of adipocytes to trap non-
248 phosphorylated glucose. Second, loss of HK2 in adipocytes de-represses glucose
249 production in liver.
250 How does loss of HK2 in adipose tissue de-repress hepatic gluconeogenesis? The
251 Kahn group showed that adipose ChREBP normally promotes synthesis of fatty acids
252 including palmitic acid hydroxy stearic acid (PAHSA) which is secreted and suppresses
253 hepatic gluconeogenesis[20]. We demonstrate that loss of HK2 impairs ChREBP activation
254 and prevents fatty acid synthesis. Thus, loss of adipose HK2 may de-represses hepatic
255 gluconeogenesis via down-regulation of circulating PAHSA.
256 In liver, insulin normally down-regulates gluconeogenesis to decrease blood glucose
257 and up-regulates lipogenesis to increase energy storage. Paradoxically, in type 2 diabetes,
258 insulin fails to inhibit gluconeogenesis but stimulates lipogenesis, hence the liver is
259 selectively insulin resistant[2]. Furthermore, previous findings suggest that selective
260 resistance occurs despite intact hepatic insulin signaling[26]. Consistent with these previous
261 findings, we observed that loss of adipose HK2 causes selective insulin resistance without
262 affecting systemic insulin signaling. Thus, we propose that loss of adipose HK2 is a
263 mechanism for selective insulin resistance and ultimately diabetes.
264 We found an HK2-R42H mutation in naturally hyperglycemic Mexican cavefish. To
265 date, no human monogenic disease has been reported associated with mutations in the *HK2*
266 gene. However, 12 R42W and 4 R42Q alleles are reported in the genomAD database[27].

267 Further studies are required to determine whether these alleles are loss-of-function and
268 associated with diabetes.
269
270 **Methods**
271 **Mouse**
272 Wild-type C57BL/6JRj mice were purchased from JANVIER LABS. Mice carrying *Hk2* with
273 exons 4-10 flanked by loxP sites (*Hk2*$^{fl/fl}$) were as described[28]. *Adipoq-CreER*^{T2} mice were
274 provided by Prof. Stefan Offermanns (MPI-HLR, Germany)[29]. *Hk2*$^{fl/fl}$ mice were crossed with
275 *Adipoq-CreER*^{T2} mice, and resulting Cre positive *Hk2*$^{fl/+}$ mice were crossed with *Hk2*$^{fl/fl}$ mice
276 to generate adipocyte-specific *Hk2* knockout (*Adipoq-CreER*^{T2} positive *Hk2*$^{fl/fl}$) mice
277 (AdHk2KO). *Hk2* knockout was induced by i.p. injection of 1 mg/mouse tamoxifen (Sigma-
278 Aldrich) in corn oil for 7 days. Littermate *Cre* negative animals were used as a control.
279 Control mice were also treated with tamoxifen.
280 The (R42H) modification of the *Hk2* locus using Cas9/CRISPR was carried out by
281 electroporation of zygotes. C57BL/6J female mice underwent ovulation induction by i.p.
282 injection of 5 IU equine chorionic gonadotrophin (PMSG; Folligon–InterVet), followed by i.p.
283 injection of 5 IU human chorionic gonadotropin (Pregnyl–Essex Chemie) 48 hours later. For
284 recovery of zygotes, C57BL/6J males and females were mated immediately after
285 administration of human chorionic gonadotropin. Zygotes were collected from oviducts 24
286 hours after the human chorionic gonadotropin injection, and were then freed from any
287 remaining cumulus cells by a 1–2 min treatment of 0.1% hyaluronidase (Sigma-Aldrich)
288 dissolved in M2 medium (Sigma). Prior to electroporation, the zona pellucida was partially
289 removed by brief treatment with acid Tyrode's solution and the zygotes were washed and
290 briefly cultured in M16 (Sigma) medium at 37 °C and 5% CO_2. Electroporation with a
291 mixture of 16 uM cr:trcrRNA hybrid targeting *Hk2* (5'cccttctggagatttctaggcgg 3' - PAM
292 underlined), 16 µM Cas9 protein and 200 nt ssDNA oligonucleotide carrying the desired
293 mutations
294 (5'gcaaggctgggttatatttaataacatagaacctattcttgtcccctgcccccttttcaggttgaccagtatctctaccacatgcgtct
295 ctcagatgagacccttctggagatttctagacatttccggaaggagatggagaaggggctaggagctaccacacaccctacag
296 cagctgtgaagatgctgcccacctttgtg 3') (all reagents from IDT) was carried out using 1 mm gap
297 electroporation cuvette and the ECM830 electroporator (BTX Harvard Apparatus). Two 3
298 millisecond pulses of 30 V with 100 millisecond intervals were applied as previously
299 described[30]. Surviving zygotes were washed with M16 medium and transferred immediately
300 into the oviducts of 8–16 week old pseudopregnant Crl:CD1(ICR) females that had been
301 mated with sterile genetically vasectomized males[31] the day before zygote transfer (0.5 dpc).
302 Pregnant females were allowed to deliver and raise their pups until weaning age. In total,
303 475 zygotes were electroporated and 470 surviving zygotes were transferred into 20 foster

304 mothers. Possible lethality of NHEJ-mediated disruption of the *Hk2* locus resulted in
305 substantial reduction of offspring. Only 4 of 20 foster mothers produced live litters with a
306 total of seven F_0 pups. Two F_0 pups carrying the desired modification (R42H) of the *Hk2*
307 gene were crossed with C57BL/6JRj mice. Mice of the F_4 generation was used to determine
308 the mendelian ratio.
309 Mice were housed at 22 ºC in a conventional facility with a 12 hour light/dark cycle
310 with unlimited access to water, and normal diet (ND) or high fat diet (HFD: 60% kcal % fat
311 NAFAG 2127, KLIBA). Only male mice between 6 and 17 weeks of age were used for
312 experiments.
313
314 **Plasmids**
315 The R42H mutation was introduced into the pLenti-CMV-ratHK2 by PCR using the oligos
316 5'atttctaggcACttccggaaggagatggagaaag3' and 5'cttccggaaGTgcctagaaatctccagaagggtc3'.
317 The desired sequence change was confirmed.
318
319 **Cell culture**
320 HEK293T cells were obtained from ACTT and cultured in M1 (DMEM supplemented with 4
321 mM glutamine, 1mM sodium pyruvate, 1x penicillin and streptomycin, and 10% FBS). 3T3-
322 L1 cells were obtained from ATCC and cultured and differentiated as previously described[32].
323 In brief, 3T3-L1 preadipocyte cells were maintained in M1 medium at 37 ºC incubator with
324 5% CO_2. For differentiation, cells were maintained in M1 medium for 2 days after reaching
325 confluence. The cells were the transferred to M2 medium (M1 medium supplemented with
326 1.5 µg/mL insulin, 0.5 mM IBMX, 1 µM dexamethasone, and 2 µM rosiglitazone), defined as
327 day 0 post-differentiation. After 2 days, the cells were transferred to M3 medium (M1 with
328 1.5 µg/mL insulin). At day 4 post-differentiation, cells were transferred back to M2 medium.
329 From day 6 post-differentiation, cells were maintained in M3 with medium change every two
330 days.
331 For Hk2 knockdown, MISSION shRNA (TRCN0000280118) or control pLKO plasmid
332 were purchased from Merck and co-transfected with psPAX2 (a gift from Didier Trono:
333 Addgene plasmid # 12260) and pCMV-VSV-G[33] (a gift from Robert Weinberg: Addgene
334 plasmid # 8454) into HEK293T cells. Supernatants containing lentivirus were collected one
335 day after transfection, and used to infect undifferentiated 3T3-L1 cells. Transduced cells
336 were selected by puromycin. For all experiments, 8-14 days post-differentiated cells were
337 used.
338
339 **Human biopsies**

340 Omental white adipose tissue (oWAT) biopsies were obtained from lean subjects with
341 normal fasting glucose level and body mass index (BMI) < 27 kg/m^2, from obese non-
342 diabetic subjects with BMI > 35 kg/m^2 HbA1c < 6.0%, and from obese diabetic sujects with
343 BMI > 35 kg/m^2 HbA1c > 6.1% (**Table S2**). All subjects gave informed consent before the
344 surgical procedure. Patients were fasted overnight and underwent general anesthesia. All
345 oWAT specimens were obtained between 8:30 and 12:00am, snap-frozen in liquid nitrogen,
346 and stored at -80 ºC for subsequent use.
347
348 **Proteomics**
349 Tissues were pulverized and homogenized in lysis buffer containing 100 mM Tris-HCl pH7.5,
350 2 mM EDTA, 2 mM EGTA, 150 mM NaCl, 1% Triton X-100, cOmplete inhibitor cocktail
351 (Roche) and PhosSTOP (Roche). Proteins were precipitated by trichloroacetic acid (Sigma)
352 and the resulting protein pellets were washed with cold acetone. 25 µg of peptides were
353 labeled with isobaric tandem mass tags (TMT 10-plex, Thermo Fisher Scientific) as
354 described previously [34]. Shortly, peptides were resuspended in 20 µl labeling buffer (2 M
355 urea, 0.2 M HEPES, pH 8.3) and 5 µL of each TMT reagent were added to the individual
356 peptide samples followed by a 1 h incubation at 25 °C. To control for ratio distortion during
357 quantification, a peptide calibration mixture consisting of six digested standard proteins
358 mixed in different amounts was added to each sample before TMT labeling. To quench the
359 labelling reaction, 1.5 µL aqueous 1.5 M hydroxylamine solution was added and samples
360 were incubated for another 10 min at 25 °C followed by pooling of all samples. The pH of
361 the sample pool was increased to 11.9 by adding 1 M phosphate buffer (pH 12) and
362 incubated for 20 min at 25 °C to remove TMT labels linked to peptide hydroxyl groups.
363 Subsequently, the reaction was stopped by adding 2 M hydrochloric acid and until a pH < 2
364 was reached. Finally, peptide samples were further acidified using 5% TFA, desalted using
365 Sep-Pak Vac 1cc (50 mg) C18 cartridges (Waters) according to the manufacturer's
366 instructions and dried under vacuum.
367 TMT-labeled peptides were fractionated by high-pH reversed phase separation using
368 a XBridge Peptide BEH C18 column (3,5 µm, 130 Å, 1 mm x 150 mm, Waters) on an Agilent
369 1260 Infinity HPLC system. Peptides were loaded on column in buffer A (20 mM ammonium
370 formate in water, pH 10) and eluted using a two-step linear gradient from 2% to 10% in 5
371 minutes and then to 50% buffer B (20 mM ammonium formate in 90% acetonitrile, pH 10)
372 over 55 min at a flow rate of 42 µl/min. Elution of peptides was monitored with a UV detector
373 (215 nm, 254 nm) and a total of 36 fractions were collected, pooled into 12 fractions using a
374 post-concatenation strategy as previously described[35] and dried under vacuum.
375 Dried peptides were resuspended in 20 µl of 0.1% aqueous formic acid and
376 subjected to LC–MS/MS analysis using a Q Exactive HF Mass Spectrometer fitted with an

377 EASY-nLC 1000 (both Thermo Fisher Scientific) and a custom-made column heater set to
378 60 °C. Peptides were resolved using a RP-HPLC column (75 µm × 30 cm) packed in-house
379 with C18 resin (ReproSil-Pur C18–AQ, 1.9 µm resin; Dr. Maisch GmbH) at a flow rate of 0.2
380 µL/min. The following gradient was used for peptide separation: from 5% B to 15% B over 10
381 min to 30% B over 60 min to 45 % B over 20 min to 95% B over 2 min followed by 18 min at
382 95% B. Buffer A was 0.1% formic acid in water and buffer B was 80% acetonitrile, 0.1%
383 formic acid in water.
384 The mass spectrometer was operated in DDA mode with a total cycle time of
385 approximately 1 sec. Each MS1 scan was followed by high-collision-dissociation (HCD) of
386 the 10 most abundant precursor ions with dynamic exclusion set to 30 sec. For MS1, 3e6
387 ions were accumulated in the Orbitrap over a maximum time of 100 ms and scanned at a
388 resolution of 120,000 FWHM (at 200 m/z). MS2 scans were acquired at a target setting of
389 1e5 ions, accumulation time of 100 ms and a resolution of 30,000 FWHM (at 200 m/z).
390 Singly charged ions and ions with unassigned charge state were excluded from triggering
391 MS2 events. The normalized collision energy was set to 35%, the mass isolation window
392 was set to 1.1 m/z and one microscan was acquired for each spectrum.
393 The acquired raw-files were converted to the mascot generic file (mgf) format using
394 the msconvert tool (part of ProteoWizard, version 3.0.4624 (2013-6-3)). Using the MASCOT
395 algorithm (Matrix Science, Version 2.4.1), the mgf files were searched against a decoy
396 database containing normal and reverse sequences of the predicted SwissProt entries of
397 Mus musculus (www.ebi.ac.uk, release date 2014/11/24), the six calibration mix proteins[34]
398 and commonly observed contaminants (in total 50214 sequences for Mus musculus)
399 generated using the SequenceReverser tool from the MaxQuant software (Version
400 1.0.13.13). The precursor ion tolerance was set to 10 ppm and fragment ion tolerance was
401 set to 0.02 Da. The search criteria were set as follows: full tryptic specificity was required
402 (cleavage after lysine or arginine residues unless followed by proline), 3 missed cleavages
403 were allowed, carbamidomethylation (C) and TMT6plex (K and peptide N-terminus) were set
404 as fixed modification and oxidation (M) as a variable modification. Next, the database search
405 results were imported into the Scaffold Q+ software (version 4.3.2, Proteome Software Inc.,
406 Portland, OR) and the protein false identification rate was set to 1% based on the number of
407 decoy hits. Proteins that contained similar peptides and could not be differentiated based on
408 MS/MS analysis alone were grouped to satisfy the principles of parsimony. Proteins sharing
409 significant peptide evidence were grouped into clusters. Acquired reporter ion intensities in
410 the experiments were employed for automated quantification and statically analysis using a
411 modified version of our in-house developed SafeQuant R script[34]. This analysis included
412 adjustment of reporter ion intensities, global data normalization by equalizing the total
413 reporter ion intensity across all channels, summation of reporter ion intensities per protein

414 and channel, calculation of protein abundance ratios and testing for differential abundance
415 using empirical Bayes moderated t-statistics. Finally, the calculated p-values were corrected
416 for multiple testing using the Benjamini−Hochberg method (q-value). Deregulated proteins
417 were selected by log2(fold change) > 0.6 or log2(fold change) < -0.6, q-value < 0.01.
418
419 **Immunoblots**
420 Adipose tissue, liver, and skeletal muscle were homogenized in lysis buffer containing 100
421 mM Tris-HCl pH7.5, 2 mM EDTA, 2 mM EGTA, 150 mM NaCl, 1% Triton X-100, cOmplete
422 inhibitor cocktail (Roche) and PhosSTOP (Roche). Protein concentration was determined by
423 the Bradford assay, and equal amounts of protein were separated by SDS-PAGE, and
424 transferred onto nitrocellulose membranes (GE Healthcare). Antibodies used in this study
425 were as follows: AKT (Cat#4685), AKT-pS473 (Cat#4060), HK2 (Cat#2867), HK1
426 (Cat#2024), HA tag (Cat#3724) from Cell Signaling, GLUT4 (Cat# NBP2-22214, NOVUS),
427 and ACTIN (Cat#MAB1501, Millipore).
428
429 **RNA isolation and quantitative RT-PCR**
430 Total RNA was isolated with TRIzol reagent (Sigma-Aldrich) and RNeasy kit (Qiagen). RNA
431 was reverse-transcribed to cDNA using iScript cDNA synthesis kit (BIO-RAD).
432 Semiquantitative real-time PCR analysis was performed using fast SYBR green (Applied
433 Biosystems). Relative expression levels were determined by normalizing each CT values to
434 *Tbp* using the ΔΔCT method. The sequence for the primers used in this study was as
435 follows. Fasn-fw: 5'GCTGCGGAAACTTCAGGAAAT3', Fasn-rv:
436 5'AGAGACGTGTCACTCCTGGACTT3', Acc-fw: 5'AAGGCTATGTGAAGGATG3', Acc-rv:
437 5'CTGTCTGAAGAGGTTAGG3', Cd36-fw: 5' TGGCCTTACTTGGGATTGG3', Cd36-rv: 5'
438 CCAGTGTATATGTAGGCTCATCCA 3', G6pc-fw: 5'CCATGCAAAGGACTAGGAACAA3',
439 G6pc-rv: 5' TACCAGGGCCGATGTCAAC 3', Pepck-fw: 5' CCACAGCTGGTGCAGAACA3',
440 Pepck-rv: 5' GAAGGGTCGATGGCAAA 3', Chrebp-fw:
441 5'CACTCAGGGAATACACGCCTAC3', Chrebp-rv: 5'ATCTTGGTCTTAGGGTCTTCAGG3',
442 Chrebp-alpha-fw: 5'CGACACTCACCCACCTCTTC3', Chrebp-alpha-rv:
443 5'TTGTTCAGCCGGATCTTGTC3', Chrebp-beta-fw: 5'TCTGCAGATCGCGTGGAG3',
444 Chrebp-beta-rv: 5'CTTGTCCCGGCATAGCAAC3', Hk2-fw: 5'
445 ACGGAGCTCAACCAAAACCA3', Hk2-rv: 5'TCCGGAACCGCCTAGAAATC3', Foxk1-fw: 5'
446 GGCTGTCACTCAGAATGGAA3', Foxk1-rv: 5'GAGGCAGATGTGGTAGTGGAG3', Foxk2-
447 fw: 5' CCACGGGAACTATCAGTGCT3' , Foxk2-rv: 5' GTCATCCTTTGGGCTGTCTC3,
448 Adipoq-fw: 5'TGACGACACCAAAAGGGCTC3', Adipoq-rv: 5'
449 ACGTCATCTTCGGCATGACT3', aP2-fw: 5' TCGGTTCCTGAGGATACAAGAT3', aP2-rv:

450 5'TTTGATGACTGTGGGATTGAAG3', Tbp-fw: 5'TGCTGTTGGTGATTGT3', Tbp-rv:5'
451 CTTGTGTGGGAAAGAT3'.
452
453 **Hexokinase assay**
454 Measurements were performed with a hexokinase assay kit (abcam) following
455 manufacturer's instructions.
456
457 **Seahorse analyses**
458 Measurements were performed with an XF96 Extracellular Flux Analyzer (Seahorse
459 Bioscience of Agilent) following manufacturer's instructions.
460
461 **Lactate measurement**
462 Differentiated adipocytes were starved serum overnight and stimulated with 100 nM insulin
463 for 2 hours. Extracellular lactate was measured with the Lactate Pro 2 analyzer (Axonlab).
464
465 **^{3}H-2DG uptake assay**
466 Differentiated adipocytes were starved for serum for 5 hours and then incubated in Krebs
467 Ringer Phosphate Hepes (KRPH) buffer with or without 100 nM insulin for 20 min. Cells
468 were incubated with 50 μM 2DG containing 0.25 μCi ^{3}H-2-deoxyglucose (2DG, Perkin
469 Elmer) for 5 min and washed three times with cold PBS. Cells were lysed in lysis buffer and
470 cleared by centrifugation at 14,000 g for 10 min. Incorporated ^{3}H-2DG was measured with a
471 scintillation counter.
472
473 **Insulin tolerance test, glucose tolerance test, pyruvate tolerance test**
474 For the insulin and glucose tolerance tests, mice were fasted for 6 hours and insulin
475 Humalog (Lilly, i.p. 0.75 or 0.5 U/kg body weight) or glucose (2 g/kg body weight) was given,
476 respectively. For the pyruvate tolerance test, mice were fasted for 15 hours and pyruvate (2
477 g/kg body weight) was administered. Blood glucose was measured with a blood glucose
478 meter (Accu-Check).
479
480 **Polysome profile analyses**
481 Tissues were homogenized in polysome lysis buffer (10 mM Tris-HCl, pH7.5, 140 mM KCl, 5
482 mM $MgCl_2$, 1mM DTT, 0.5% Triton x-100, 0.05% sodium deoxycholate, 40 u/mL RNase
483 inhibitor) in the presence or absence of 100 μg/mL cycloheximide and the lysates were
484 centrifuged twice at 14,000 g for 10 min. The cleared lysates were loaded onto 5-50%
485 sucrose gradients (10 mM Tris-HCl, pH7.5, 140 mM KCl, 5 mM $MgCl_2$, 5% or 50% sucrose)
486 and centrifuged with TH-641 (Thermo Scientific) at 36,000 rpm for 2 hours at 4 ºC. Fractions

487 were collected by a Gradient Station (BIOCOMP INSTRUMENTS) with continuous recording
488 of optical density (OD) at 254 nm. RNA from each fraction was isolated with TRIzol and
489 qRT-PCR were performed as described[36].
490
491 **Insulin ELISA**
492 Plasma insulin levels were measured by ultrasensitive mouse insulin ELISA kit (Crystal
493 Chem) according to the manufacturer's instructions.
494
495 **Hepatic triglyceride measurement**
496 Hepatic triglyceride levels were measured using a triglyceride assay kit (Abcam) according
497 to the manufacturer's instructions.
498
499 **Body composition measurement**
500 Body composition was measured by nuclear magnetic resonance imaging (Echo Medical
501 Systems).
502
503 **Study Approval**
504 All animal experiments were performed in accordance with federal guidelines for animal
505 experimentation and were approved by the Kantonales Veterinäramt of the Kanton Basel-
506 Stadt. For human biopsies, the study protocol was approved by the Ethikkomission
507 Nordwest- und Zentralschweiz (EKNZ).
508
509 **Statistics**
510 Sample size was chosen according to our previous studies and published reports in which
511 similar experimental procedures were described. The investigators were not blinded to the
512 treatment groups. All data are shown as the mean ± SEM. Sample numbers are indicated
513 in each figure legend. For mouse experiments, *n* represents the number of animals, and for
514 cell culture experiments, *N* indicates the number of independent experiments. To determine
515 the statistical significance between 2 groups, an unpaired two-tailed Student's t test was
516 performed. For more than 3 groups, one-way ANOVA was performed. For ITT, GTT, PTT,
517 weigh curve data, two-way ANOVA was performed. All statistical analysis was performed
518 using GraphPad Prism 8 (GraphPad Software). A *p* value of less than 0.05 was considered
519 statistically significant.
520
521 **Acknowledgements**
522 We thank Stefan Offermanns (MPI-HLR, Germany), Didier Trono (EPFL, Switzerland),
523 Robert Weinberg (MIT, USA), Christine Riggenbach (St. Claraspital), Christoph Handschin

(Biozentrum), the Imaging Core Facility (Biozentrum), and the Proteomics Core Facility (Biozentrum) for providing reagents and technical support. We acknowledge support from the Swiss National Science Foundation (project 179569 and NCCR 182880 to MNH and 161510 to MS), The Louis Jeantet Foundation (MNH), and the Canton of Basel (MNH). The authors declare no competing financial interests.

Contributions

MS and MNH conceived the project and designed research with additional contributions from TM and NR. MS, SS, ICF, DW, ND, AT, DR, NR performed experiments and analyzed data. NH provided reagents and mice. BKW, ACM, and RP contributed to the collection of human adipose tissue biopsies. MS and MNH wrote the manuscript.

538 **References**

539 1 Petersen, M. C. & Shulman, G. I. Mechanisms of Insulin Action and Insulin
540 Resistance. *Physiol Rev* **98**, 2133-2223, doi:10.1152/physrev.00063.2017 (2018).
541 2 Brown, M. S. & Goldstein, J. L. Selective versus total insulin resistance: a pathogenic
542 paradox. *Cell Metab* **7**, 95-96, doi:10.1016/j.cmet.2007.12.009 (2008).
543 3 Wasserman, D. H. Four grams of glucose. *Am J Physiol Endocrinol Metab* **296**, E11-
544 21, doi:10.1152/ajpendo.90563.2008 (2009).
545 4 Jackson, R. A., Roshania, R. D., Hawa, M. I., Sim, B. M. & DiSilvio, L. Impact of
546 glucose ingestion on hepatic and peripheral glucose metabolism in man: an analysis
547 based on simultaneous use of the forearm and double isotope techniques. *J Clin*
548 *Endocrinol Metab* **63**, 541-549, doi:10.1210/jcem-63-3-541 (1986).
549 5 Kowalski, G. M. & Bruce, C. R. The regulation of glucose metabolism: implications
550 and considerations for the assessment of glucose homeostasis in rodents. *Am J*
551 *Physiol Endocrinol Metab* **307**, E859-871, doi:10.1152/ajpendo.00165.2014 (2014).
552 6 Abel, E. D. *et al.* Adipose-selective targeting of the GLUT4 gene impairs insulin
553 action in muscle and liver. *Nature* **409**, 729-733, doi:10.1038/35055575 (2001).
554 7 Shepherd, P. R. *et al.* Adipose cell hyperplasia and enhanced glucose disposal in
555 transgenic mice overexpressing GLUT4 selectively in adipose tissue. *J Biol Chem*
556 **268**, 22243-22246 (1993).
557 8 Jiang, Z. Y. *et al.* Insulin signaling through Akt/protein kinase B analyzed by small
558 interfering RNA-mediated gene silencing. *Proc Natl Acad Sci U S A* **100**, 7569-7574,
559 doi:10.1073/pnas.1332633100 (2003).
560 9 Beg, M., Abdullah, N., Thowfeik, F. S., Altorki, N. K. & McGraw, T. E. Distinct Akt
561 phosphorylation states are required for insulin regulated Glut4 and Glut1-mediated
562 glucose uptake. *Elife* **6**, doi:10.7554/eLife.26896 (2017).
563 10 Cybulski, N., Polak, P., Auwerx, J., Ruegg, M. A. & Hall, M. N. mTOR complex 2 in
564 adipose tissue negatively controls whole-body growth. *Proc Natl Acad Sci U S A* **106**,
565 9902-9907, doi:10.1073/pnas.0811321106 (2009).
566 11 Kumar, A. *et al.* Fat cell-specific ablation of rictor in mice impairs insulin-regulated fat
567 cell and whole-body glucose and lipid metabolism. *Diabetes* **59**, 1397-1406,
568 doi:10.2337/db09-1061 (2010).
569 12 Shearin, A. L., Monks, B. R., Seale, P. & Birnbaum, M. J. Lack of AKT in adipocytes
570 causes severe lipodystrophy. *Mol Metab* **5**, 472-479,
571 doi:10.1016/j.molmet.2016.05.006 (2016).
572 13 Tang, Y. *et al.* Adipose tissue mTORC2 regulates ChREBP-driven de novo
573 lipogenesis and hepatic glucose metabolism. *Nat Commun* **7**, 11365,
574 doi:10.1038/ncomms11365 (2016).
575 14 Tan, S. X. *et al.* Selective insulin resistance in adipocytes. *J Biol Chem* **290**, 11337-
576 11348, doi:10.1074/jbc.M114.623686 (2015).
577 15 Shimobayashi, M. *et al.* Insulin resistance causes inflammation in adipose tissue. *J*
578 *Clin Invest* **128**, 1538-1550, doi:10.1172/JCI96139 (2018).
579 16 Ducluzeau, P. H. *et al.* Regulation by insulin of gene expression in human skeletal
580 muscle and adipose tissue. Evidence for specific defects in type 2 diabetes. *Diabetes*
581 **50**, 1134-1142, doi:10.2337/diabetes.50.5.1134 (2001).
582 17 Riddle, M. R. *et al.* Insulin resistance in cavefish as an adaptation to a nutrient-limited
583 environment. *Nature* **555**, 647-651, doi:10.1038/nature26136 (2018).
584 18 Nawaz, M. H. *et al.* The catalytic inactivation of the N-half of human hexokinase 2
585 and structural and biochemical characterization of its mitochondrial conformation.
586 *Biosci Rep* **38**, doi:10.1042/BSR20171666 (2018).
587 19 Heikkinen, S. *et al.* Hexokinase II-deficient mice. Prenatal death of homozygotes
588 without disturbances in glucose tolerance in heterozygotes. *J Biol Chem* **274**, 22517-
589 22523, doi:10.1074/jbc.274.32.22517 (1999).

20 Vijayakumar, A. *et al.* Absence of Carbohydrate Response Element Binding Protein in Adipocytes Causes Systemic Insulin Resistance and Impairs Glucose Transport. *Cell Rep* **21**, 1021-1035, doi:10.1016/j.celrep.2017.09.091 (2017).

21 Horton, J. D., Goldstein, J. L. & Brown, M. S. SREBPs: activators of the complete program of cholesterol and fatty acid synthesis in the liver. *J Clin Invest* **109**, 1125-1131, doi:10.1172/JCI15593 (2002).

22 Ortega-Prieto, P. & Postic, C. Carbohydrate Sensing Through the Transcription Factor ChREBP. *Front Genet* **10**, 472, doi:10.3389/fgene.2019.00472 (2019).

23 Herman, M. A. *et al.* A novel ChREBP isoform in adipose tissue regulates systemic glucose metabolism. *Nature* **484**, 333-338, doi:10.1038/nature10986 (2012).

24 Li, M. V. *et al.* Glucose-6-phosphate mediates activation of the carbohydrate responsive binding protein (ChREBP). *Biochem Biophys Res Commun* **395**, 395-400, doi:10.1016/j.bbrc.2010.04.028 (2010).

25 Sukonina, V. *et al.* FOXK1 and FOXK2 regulate aerobic glycolysis. *Nature* **566**, 279-283, doi:10.1038/s41586-019-0900-5 (2019).

26 Titchenell, P. M. *et al.* Direct Hepatocyte Insulin Signaling Is Required for Lipogenesis but Is Dispensable for the Suppression of Glucose Production. *Cell Metab* **23**, 1154-1166, doi:10.1016/j.cmet.2016.04.022 (2016).

27 Karczewski, K. J. *et al.* Variation across 141,456 human exomes and genomes reveals the spectrum of loss-of-function intolerance across human protein-coding genes. *bioRxiv*, 531210, doi:10.1101/531210 (2019).

28 Patra, K. C. *et al.* Hexokinase 2 is required for tumor initiation and maintenance and its systemic deletion is therapeutic in mouse models of cancer. *Cancer Cell* **24**, 213-228, doi:10.1016/j.ccr.2013.06.014 (2013).

29 Sassmann, A., Offermanns, S. & Wettschureck, N. Tamoxifen-inducible Cre-mediated recombination in adipocytes. *Genesis* **48**, 618-625, doi:10.1002/dvg.20665 (2010).

30 Chen, S., Lee, B., Lee, A. Y., Modzelewski, A. J. & He, L. Highly Efficient Mouse Genome Editing by CRISPR Ribonucleoprotein Electroporation of Zygotes. *J Biol Chem* **291**, 14457-14467, doi:10.1074/jbc.M116.733154 (2016).

31 Haueter, S. *et al.* Genetic vasectomy-overexpression of Prm1-EGFP fusion protein in elongating spermatids causes dominant male sterility in mice. *Genesis* **48**, 151-160, doi:10.1002/dvg.20598 (2010).

32 Zebisch, K., Voigt, V., Wabitsch, M. & Brandsch, M. Protocol for effective differentiation of 3T3-L1 cells to adipocytes. *Anal Biochem* **425**, 88-90, doi:10.1016/j.ab.2012.03.005 (2012).

33 Stewart, S. A. *et al.* Lentivirus-delivered stable gene silencing by RNAi in primary cells. *RNA* **9**, 493-501 (2003).

34 Ahrne, E. *et al.* Evaluation and Improvement of Quantification Accuracy in Isobaric Mass Tag-Based Protein Quantification Experiments. *J Proteome Res* **15**, 2537-2547, doi:10.1021/acs.jproteome.6b00066 (2016).

35 Wang, Y. *et al.* Reversed-phase chromatography with multiple fraction concatenation strategy for proteome profiling of human MCF10A cells. *Proteomics* **11**, 2019-2026, doi:10.1002/pmic.201000722 (2011).

36 Panda, A. C., Martindale, J. L. & Gorospe, M. Polysome Fractionation to Analyze mRNA Distribution Profiles. *Bio Protoc* **7**, doi:10.21769/BioProtoc.2126 (2017).

Fig. 1

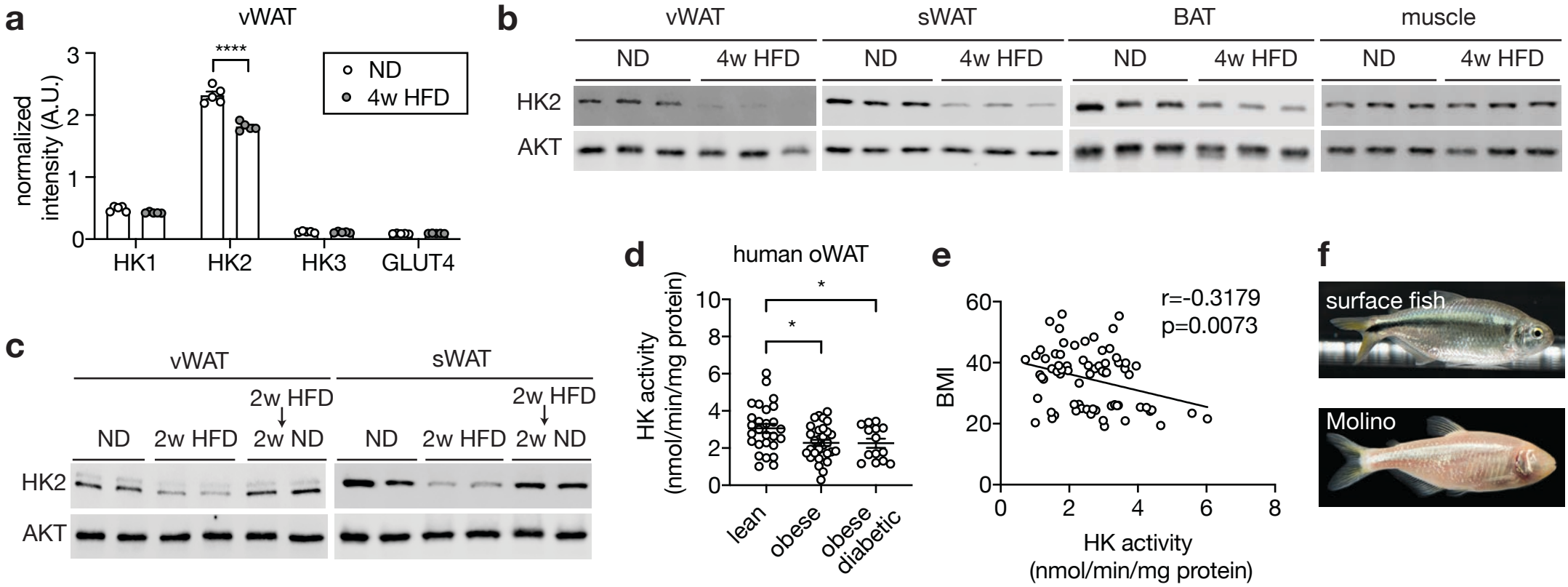

g

	hyperglycemia	insulin receptor	AKT-pS473
surface fish	-	WT	normal
cavefish Tinaja	+	P211L	impaired
cavefish Pachon	+	P211L	impaired
cavefish Molino	++	WT	normal

h

```
LSDETLLEIS KRFRKEMEKG human
LSDETLLEIS RRFRKEMEKG rat
LSDETLLEIS RRFRKEMEKG mouse
LSEDTLQEVS ERFRKEMEKG chicken
LSDETLLEVS SRFEKQMEKG frog
LSNENLMDVS KRFRKEMDKG zebrafish
LSEENLMDVS RRFRREMDKG surface fish
LSEENLMDVS RHFRREMDKG cave fish molino
31                    50
```

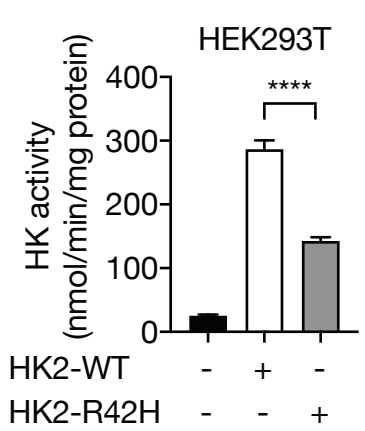

Fig. 1. Loss of HK2 in obese mouse, human, and cavefish Molino.
a. The protein levels of Hexokinases and GLUT4 in visceral white adipose tissue (vWAT) of normal diet (ND)- and 4-week high fat diet (HFD)-fed wild-type C57BL/6JRj mice. Multiple t test, ****$p<0.0001$. n=5 (ND) and 5 (HFD).
b. Immunoblots of vWAT, subcutaneous WAT (sWAT), brown adipose tissue (BAT), and skeletal muscle from ND- and 4-week HFD-fed mice. AKT serves as a loading control. n=5 (ND) and 5 (HFD).
c. Immunoblots of vWAT and sWAT from ND-, 2-week HFD-, and 2-week HFD + 2-week ND-fed mice. n=5 (ND), 5 (HFD), and 6 (HFD+ND).
d. HK activity of omental WAT (oWAT) from lean, obese, and obese diabetic patients. Two-way ANOVA, *$p<0.05$. n=27 (lean), 30 (obese), and 14 (obese diabetic).
e. HK activity positively correlated with BMI. Pearson's correlation analysis.
f. Surface fish and Mexican cavefish Molino.
g. Comparisons of phenotypes in surface fish, Pachón, Tinaja, and Molino[17].
h. Amino acid sequence alignment of the HK2-R42H mutation within vertebrates.
i. HK activity for lysates of HEK293T cells expressing control, HK2-WT, or HK2-R42H. Student's t test, ****$p<0.0001$. N=4.

Fig. 2

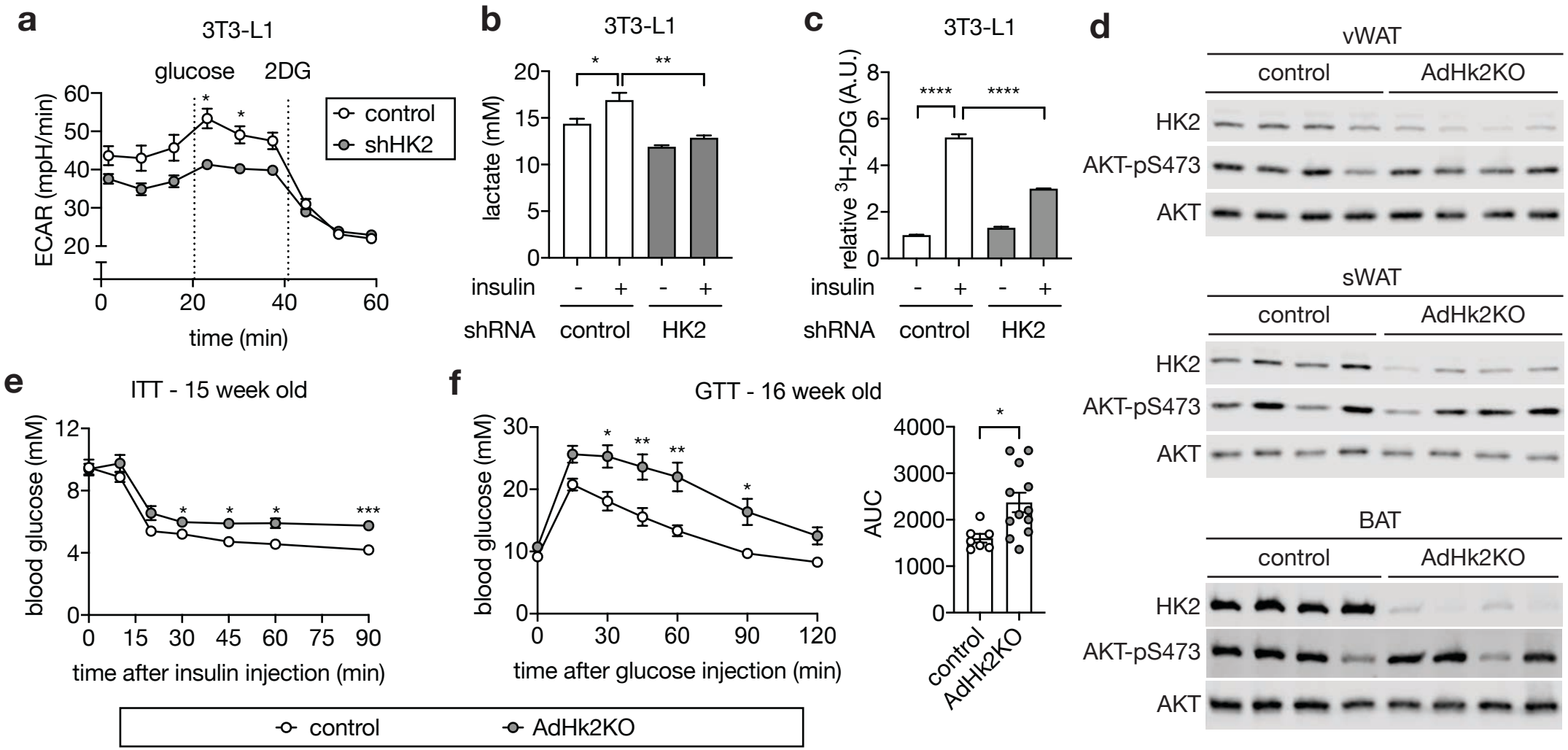
a
3T3-L1
glucose
2DG
ECAR (mpH/min)
time (min)
control
shHK2
b
3T3-L1
lactate (mM)
insulin
shRNA
control
HK2
c
3T3-L1
relative ^{3}H-2DG (A.U.)
insulin
shRNA
control
HK2
d
vWAT
sWAT
BAT
control
AdHk2KO
HK2
AKT-pS473
AKT
e
ITT - 15 week old
blood glucose (mM)
time after insulin injection (min)
f
GTT - 16 week old
blood glucose (mM)
time after glucose injection (min)
AUC
control
AdHk2KO

Fig. 2. Loss of adipose HK2 causes glucose intolerance.
a. Extracellular acidification rate of control and HK2 knockdown 3T3-L1 adipocytes in response to glucose (10 mM) and 2-deoxyglucose (2DG, 50 mM). N=8.
b. Lactate secreted into media by control and HK2 knockdown 3T3-L1 adipocytes treated with or without 100 nM insulin. N=3.
c. 2DG uptake in control and HK2 knockdown 3T3-L1 adipocytes treated with or without 100 nM insulin. N=3.
d. Immunoblots of vWAT, sWAT, and BAT of control and adipocyte-specific Hk2 knockout (AdHk2KO) mice. n=10.
e. Insulin tolerance test (ITT) on control and AdHk2KO mice. The mice were fasted for 6 hours and injected with insulin (0.5 U/kg body weight). Two-way ANOVA. *$p<0.05$, ***$p<0.001$. n=6 (control) and 10 (AdHk2KO).
f. Gucose tolerance test (GTT) on control and AdHk2KO mice. Mice were fasted for 6 hours and injected with glucose (2 g/kg body weight). Two-way ANOVA for glucose curves and Student's t test for AUC. *$p<0.05$, **$p<0.01$. n=7 (control) and 12 (AdHk2KO).

Fig. 3

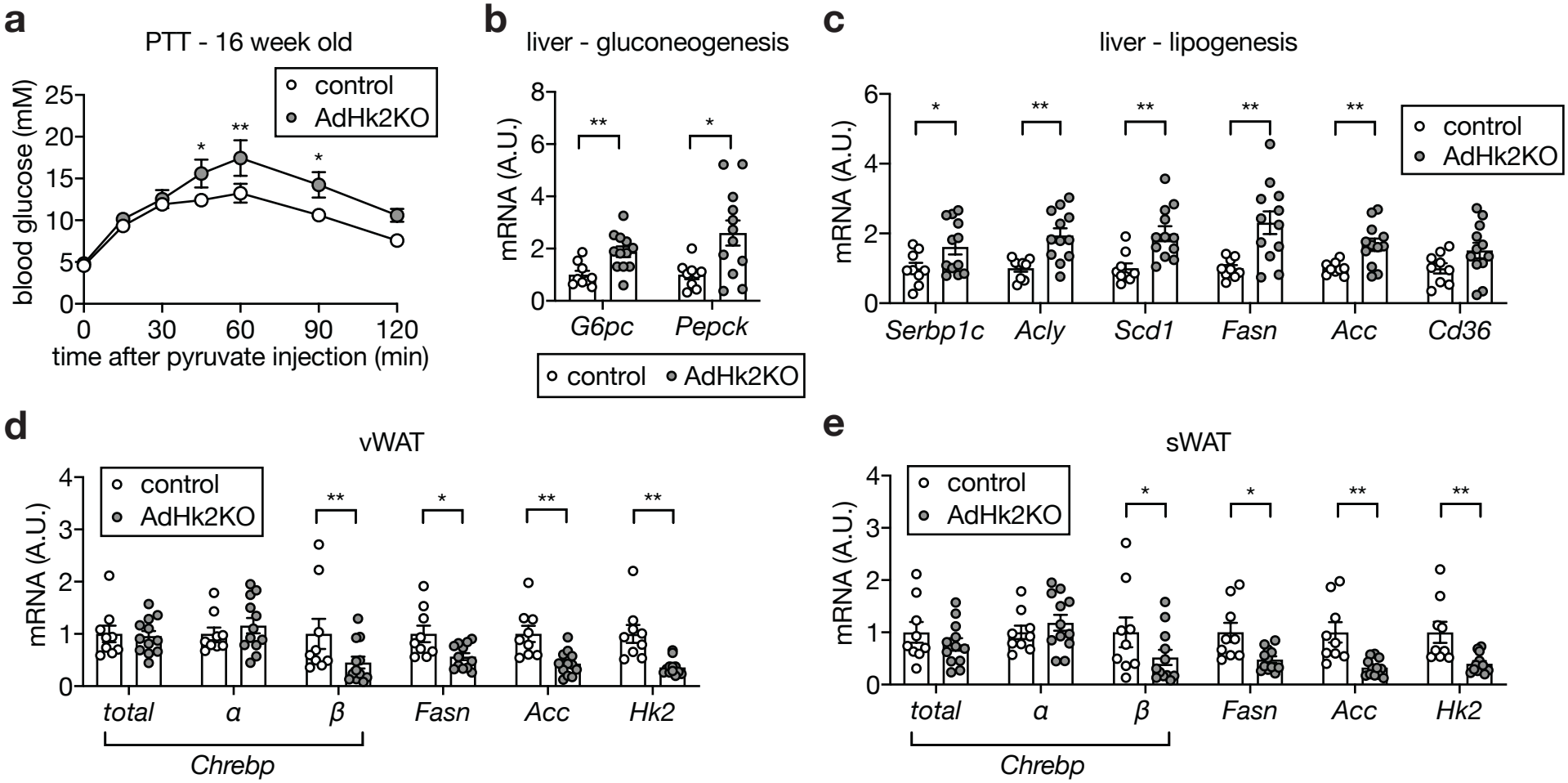
a
PTT - 16 week old
control
AdHk2KO
blood glucose (mM)
time after pyruvate injection (min)
b
liver - gluconeogenesis
mRNA (A.U.)
G6pc
Pepck
control
AdHk2KO
c
liver - lipogenesis
mRNA (A.U.)
Serbp1c
Acly
Scd1
Fasn
Acc
Cd36
control
AdHk2KO
d
vWAT
mRNA (A.U.)
control
AdHk2KO
total
α
β
Fasn
Acc
Hk2
Chrebp
e
sWAT
mRNA (A.U.)
control
AdHk2KO
total
α
β
Fasn
Acc
Hk2
Chrebp

Fig. 3. HK2 promotes ChREBP-mediated lipogenesis in adipose tissue and suppresses hepatic gluconeogenesis.

a. Pyruvate tolerance test (PTT) on control and AdHk2KO mice. Mice were fasted for 15 hours and injected with pyruvate (2 g/kg body weight). Two-way ANOVA, *$p<0.05$, **$p<0.01$. n=5 (control) and 6 (AdHk2KO).

b. mRNA levels of gluconeogenic genes in liver of control and AdHk2KO mice. Multiple t test, *$p<0.05$, **$p<0.01$. n=9 (control) and 12 (AdHk2KO).

c. mRNA levels of fatty acid synthesis genes in liver from control and AdHk2KO mice. Multiple t test, *$p<0.05$, **$p<0.01$. n=9 (control) and 12 (AdHk2KO).

d-e. mRNA levels of fatty acid synthesis genes in vWAT (d) and sWAT (e) from control and AdHk2KO mice. Multiple t test, *$p<0.05$, **$p<0.01$. n=9 (control) and 12 (AdHk2KO).

Fig. 4

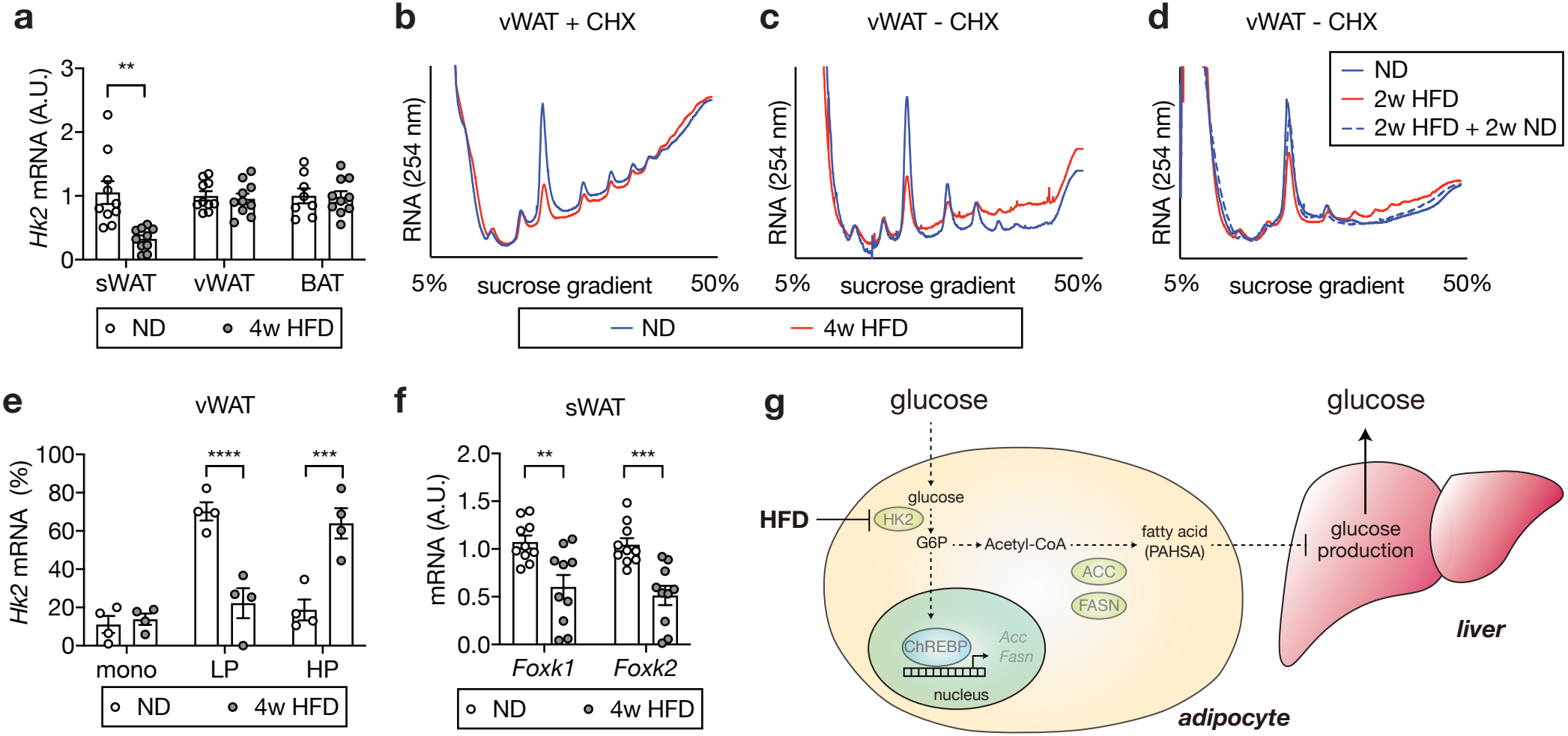
a
Hk2 mRNA (A.U.)
3
2
1
0
**
sWAT
vWAT
BAT
ND
4w HFD
b
vWAT + CHX
RNA (254 nm)
5%
sucrose gradient
50%
ND
4w HFD
c
vWAT - CHX
RNA (254 nm)
5%
sucrose gradient
50%
d
vWAT - CHX
RNA (254 nm)
5%
sucrose gradient
50%
ND
2w HFD
2w HFD + 2w ND
e
vWAT
Hk2 mRNA (%)
100
80
60
40
20
0
****
***
mono
LP
HP
ND
4w HFD
f
sWAT
mRNA (A.U.)
2.0
1.5
1.0
0.5
0.0
**
***
Foxk1
Foxk2
ND
4w HFD
g
glucose
glucose
HFD
HK2
glucose
G6P
Acetyl-CoA
fatty acid
(PAHSA)
ACC
FASN
ChREBP
Acc
Fasn
nucleus
adipocyte
glucose
production
liver

Fig. 4. Mechanism of HFD-induced HK2 down-regulation in adipose tissue.
a. *Hk2* mRNA levels in sWAT, vWAT, and BAT from ND- and 4-week HFD-fed mice. Student's t test, **p<0.01. n=10 (sWAT from ND and HFD), 10 (vWAT from ND and HFD), 8 (BAT from ND), 10 (BAT from HFD).
b. Representative polysome profiles of vWAT from ND- and 4-week HFD-fed mice. Tissue lysates were prepared in the presence of cycloheximide (CHX) to prevent ribosome run-off. n=6 (ND) and 6 (HFD).
c. Representative run-off polysome profiles of vWAT from ND- and 4-week HFD-fed mice. Tissue lysates were prepared in the absence of CHX to allow run-off. n=7 (ND) and 7 (HFD).
d. Representative run-off polysome profiles of vWAT from ND-, 2-week HFD-, 2-week HFD + 2-week ND-fed mice. Tissue lysates were prepared in the absence of CHX. n=5 (ND) and 5 (HFD).
e. *Hk2* mRNA abundance in monosome (mono), light polysome (LP), and heavy polysome (HP) fractions obtained in c. Two-way ANOVA, ***p<0.001, ****p<0.0001. n=4.
f. *Foxk1* and *Foxk2* mRNA levels in sWAT from ND- or 4-week HFD-fed mice. Multiple t test, **p<0.01, ***p<0.001. n=10 (ND) and 10 (HFD).
g. Diet-induced loss of adipose HK2 triggers hyperglycemia via reduced glucose clearance in adipocytes (left) and de-repressed hepatic gluconeogenesis (right).

Extended Data Fig. 1

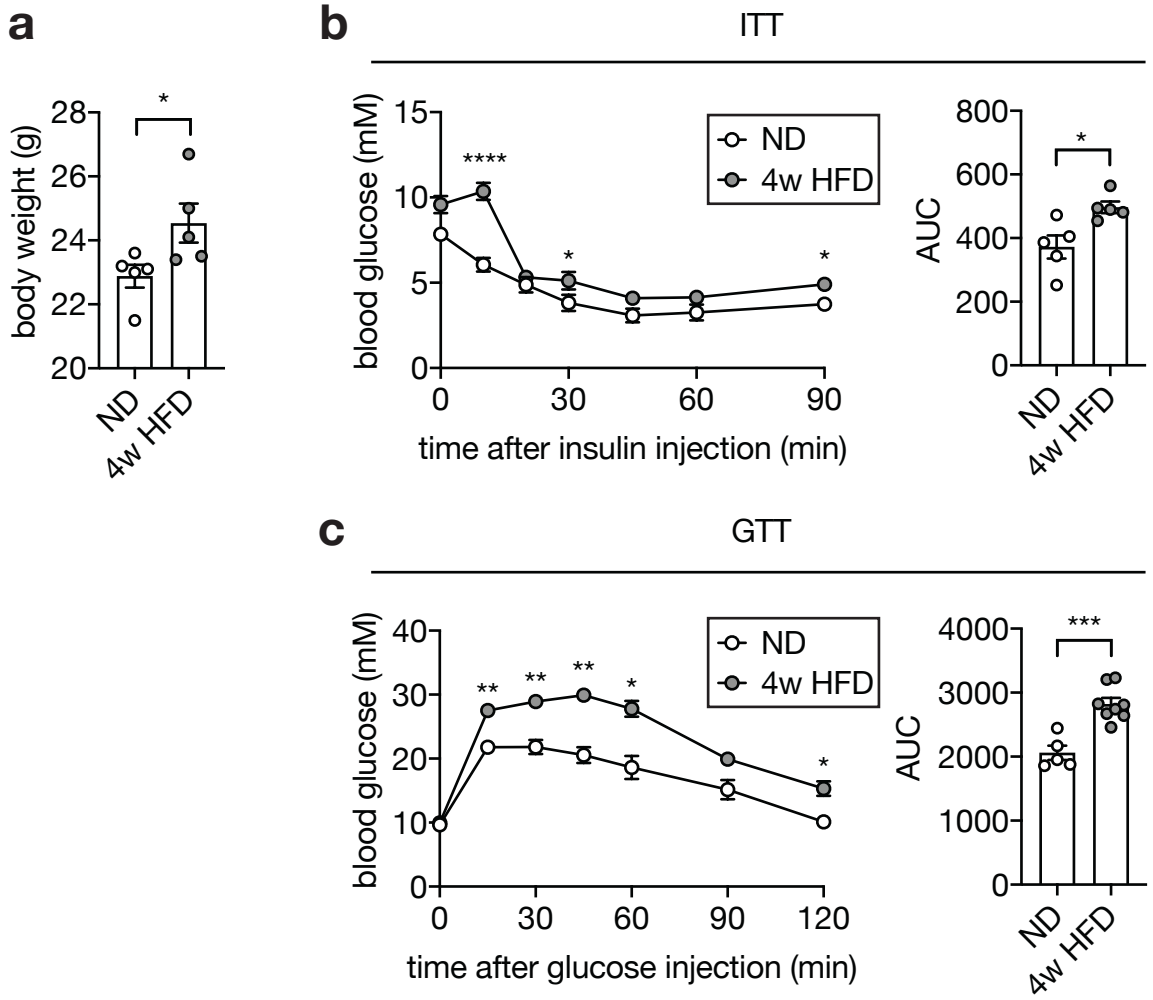

Extended Data Fig. 1. HFD-fed mice are obese, insulin resistant, and glucose intolerant.
a. Body weight of normal diet (ND)- and 4-week high fat diet (HFD)-fed wild-type C57BL/6JRj mice. Student's t test, *p<0.05. n=5 (ND) and 5 (HFD).
b. Insulin tolerance test (ITT) on ND- and 4-week HFD-fed wild-type C57BL/6JRj mice. The mice were fasted for 6 hours and injected with insulin (0.5 U/kg body weight). Two-way ANOVA for glucose curves and Student's t test for AUC. *p<0.05, ****p<0.0001. n=5 (ND) and 5 (HFD).
c. Glucose tolerance test (GTT) on 4-week HFD- and ND-fed wild-type C57BL/6JRj mice. Mice were fasted for 6 hours and i.p. injected with glucose (2 g/kg body weight). Two-way ANOVA for glucose curves and Student's t test for AUC. *p<0.05, **p<0.01, ***p<0.001. n=5 (ND) and 8 (HFD).

Extended Data Fig. 2

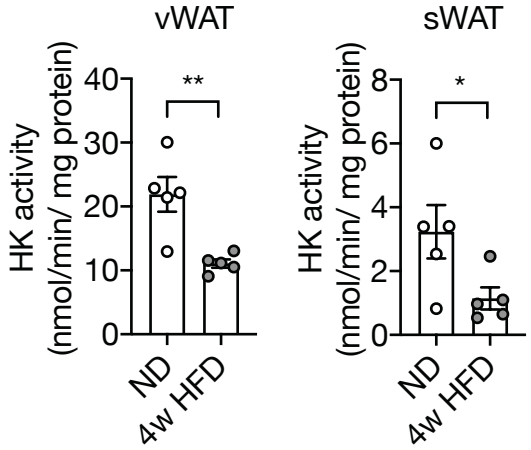

Extended Data Fig. 2.
Hexokinase (HK) activity of vWAT and sWAT from ND- and 4-week HFD-fed mice. Student's t test, *p<0.05, **p<0.01. n=5 (ND) and 5 (HFD).

Extended Data Fig. 3

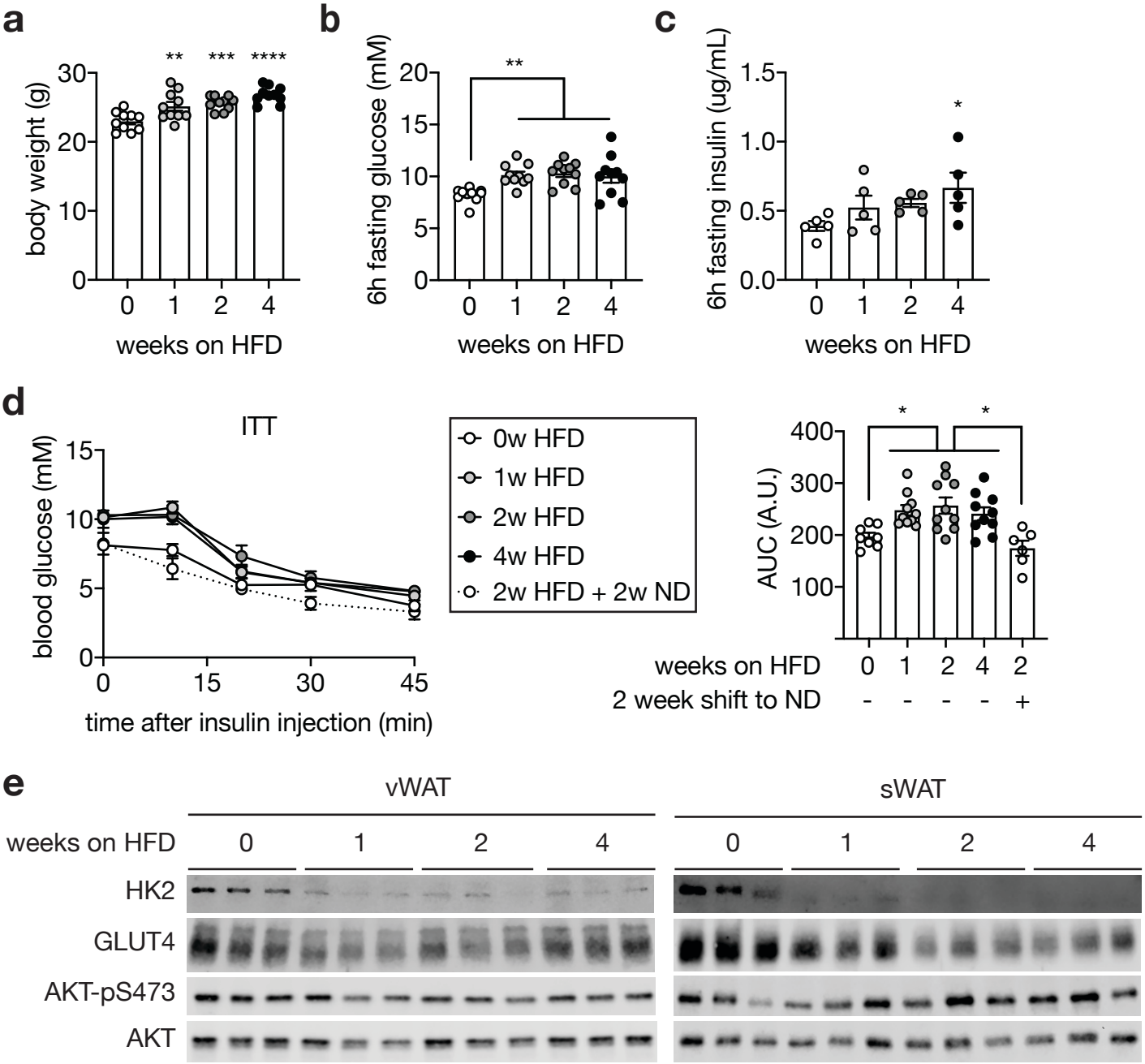

Extended Data Fig.3. Adipose HK2 expression correlates hyperglycemia.
a, **b**. Body weight (a) and fasting glucose levels (b) of mice fed a HFD for 0, 1, 2, or 4 weeks. One-way ANOVA compared to 0-week HFD-fed mice, **p<0.01, ***p<0.001. n=10
c. Fasting insulin levels of mice fed a HFD for 0, 1, 2, or 4 weeks. One-way ANOVA compared to 0-week HFD-fed mice, *p<0.05. n=5
d. ITT on mice fed a HFD for 0, 1, 2, 4 weeks, and mice fed 2-week HFD and 2week ND. The mice were fasted for 6 hours and injected with insulin (0.75 U/kg body weight). Oneway ANOVA, *p<0.05. n=10 (0-week ND), 10(1-week HFD), 10 (2-week HFD), 10 (2-week HFD), and 6 (2-week HFD + 2-week ND).
e. Immunoblots of vWAT and sWAT from mice fed a HFD for 0, 1, 2, or 4 weeks. Mice were fasted for 6 hours and injected with insulin (0.75 U/kg body weight). n=5.

Extended Data Fig. 4

a

```
5′-AGG CGC TTC-3′  Surface
5′-AGG CGC TTC-3′  Pachón
5′-AGG CGC TTC-3′  Tinaja
5′-AGG CAC TTC-3′  Molino
```

b

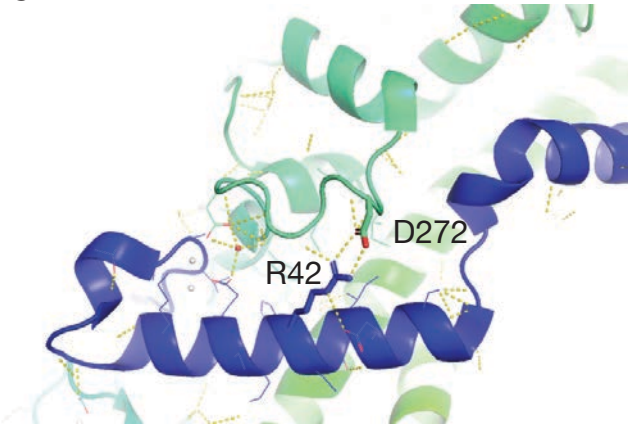

c

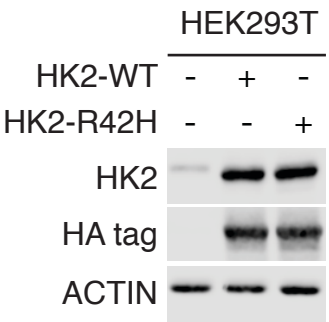

Extended Data Fig. 4. The biological significance of Arginine 42 in HK2.
a. DNA sequence of the Molino mutation.
b. Structural analyses revealed the presence of a salt bridge between Arginine 42 (R42) and Aspartic acid 272 (D272) in the human HK2 (PDB:2NTZ).
c. Immunoblots for lysates of HEK293T cells expressing control, HK2-WT, or HK2-R42H. N=4.

Extended Data Fig. 5

a

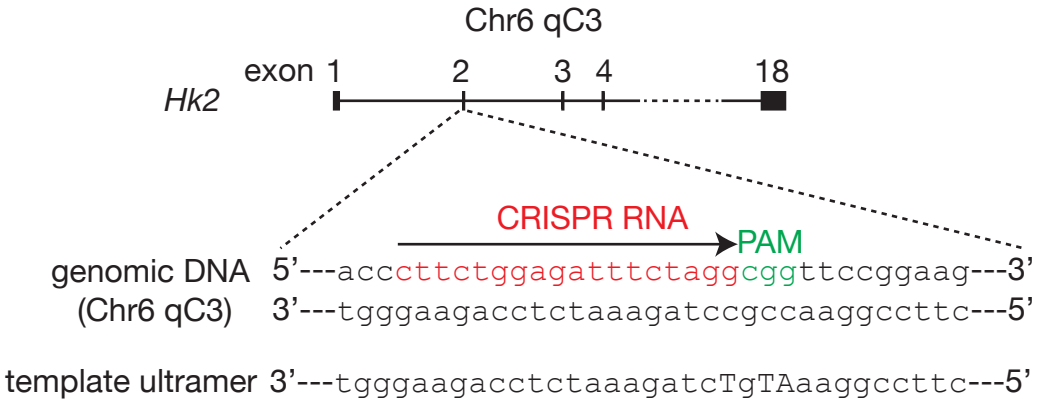

b

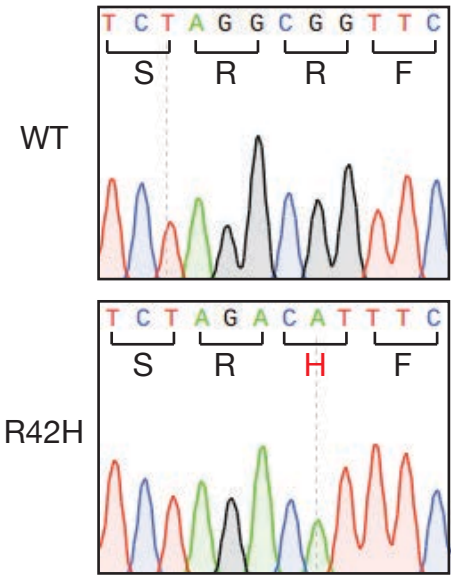

Extended Data Fig. 5. Generation of HK2-R42H knock-in mice.
a. Sequences of genomic DNA encoding R42H, CRISPR RNA, and template ultramer surrounding of the R42.
b. Sequence chromatograms of wild-type HK2 and R42H knock-in alleles.

Extended Data Fig. 6

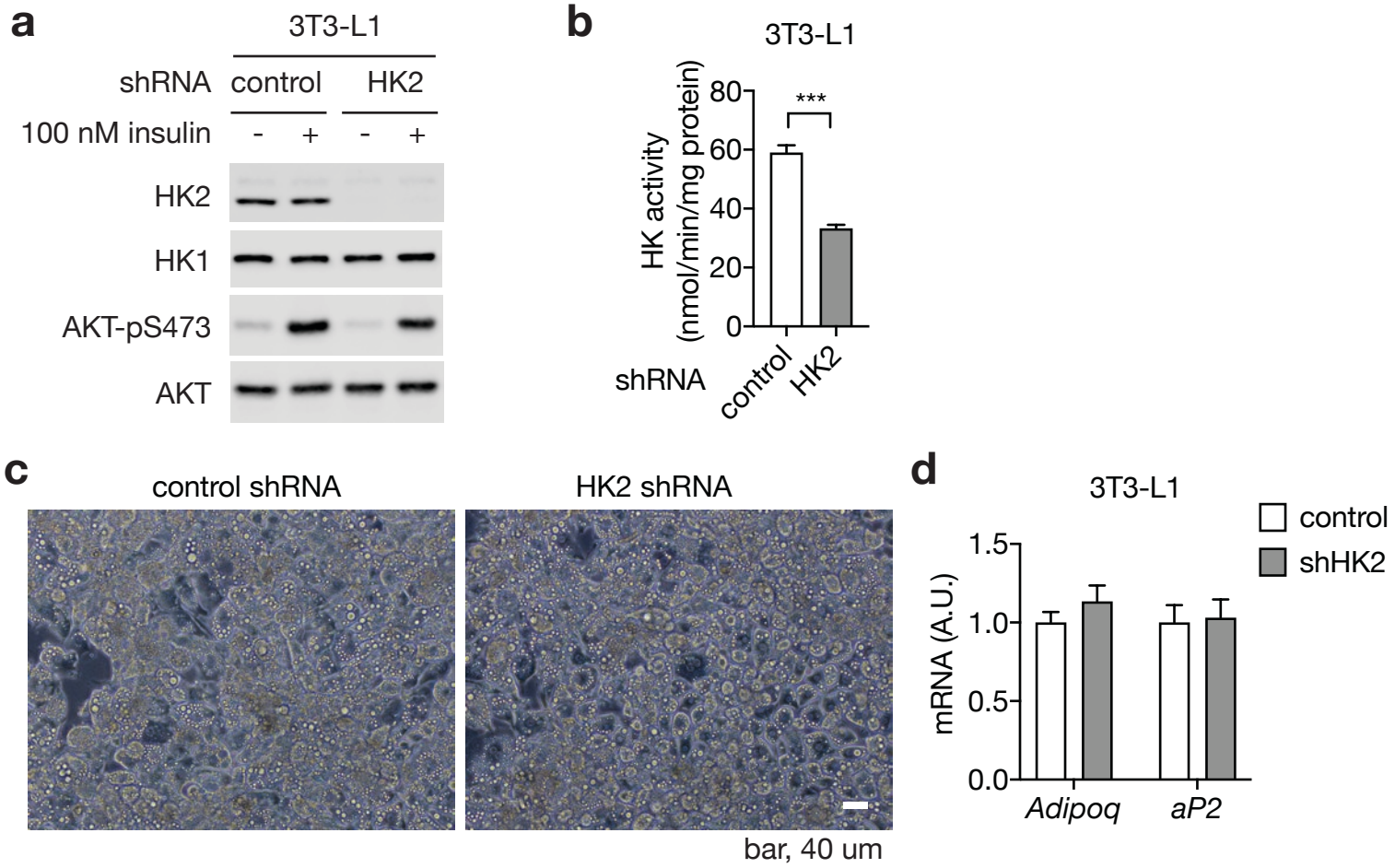

Extended Data Fig. 6. Generation and characterization of HK2 knockdown 3T3-L1 adipocytes.
a. Immunoblots of control and HK2 knockdown 3T3-L1 adipocytes. Cells were stimulated with 100 nM insulin for 25 min. N=4.
b. Hexokinase (HK) activity of control and HK2 knockdown 3T3-L1 adipocytes. Student's t test, ***$p<0.001$. N=3.
c. Bright filed images of control and HK2 knockdown 3T3-L1 adipocytes.
d. mRNA levels of mature adipocyte markers in control and HK2 knockdown 3T3-L1 adipocytes. No significant difference in multiple t test. N=3.

Extended Data Fig. 7

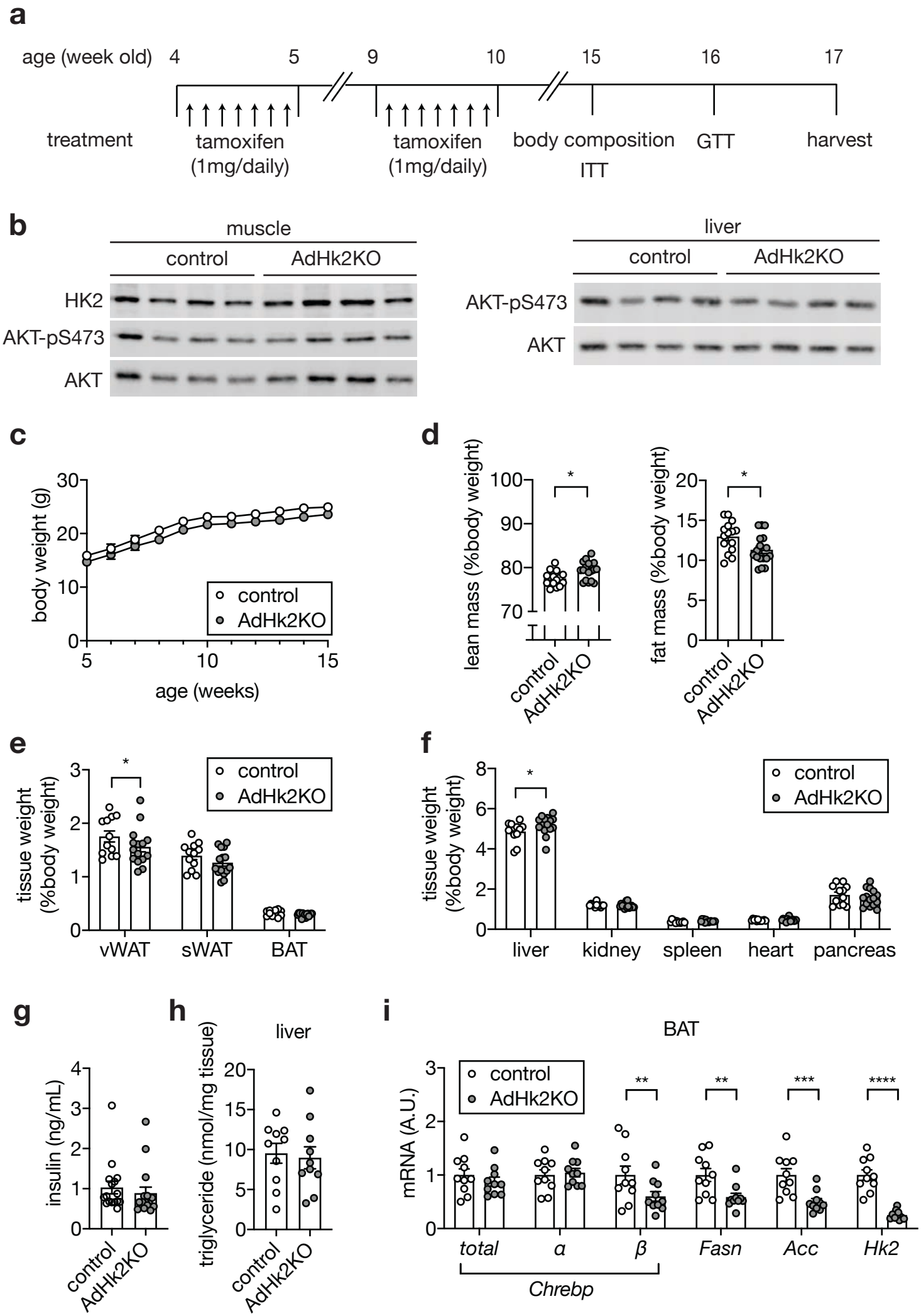

Extended Data Fig. 7. Characterization of AdHk2KO mice.

a. Experimental design of tamoxifen treatment, body composition measurement, ITT, and GTT in control and AdHk2KO mice for Fig. 2d-f. Both control and AdHk2KO mice were treated with tamoxifen.

b. Immunoblots of muscle and liver of control and AdHk2KO mice. n=5 (control) and 5 (AdHk2KO). n=10

c-d. Body weight curve (c), lean and fat mass (d) of control and AdHk2KO mice. Student's t test, *$p<0.05$. n=15 (control) and 17 (AdHk2KO).

e-f. Organ weight for fat tissues (e) and non-fat tissues (f) of control and AdHk2KO mice. Student's t test, *$p<0.05$. n=12 (control) and 15 (AdHk2KO).

g. Plasma insulin levels of ad libitum fed control and AdHk2KO mice. n=16 (control) and 16 (AdHk2KO).

h. Hepatic triglyceride levels of control and AdHk2KO mice. n=10 (control) and 10 (AdHk2KO).

i. mRNA levels of fatty acid synthesis genes in BAT from control and AdHk2KO mice. Multiple t test, **$p<0.01$, ***$p<0.001$, ****$p<0.0001$. n=10 (control) and 10 AdHk2KO).

Extended Data Fig. 8

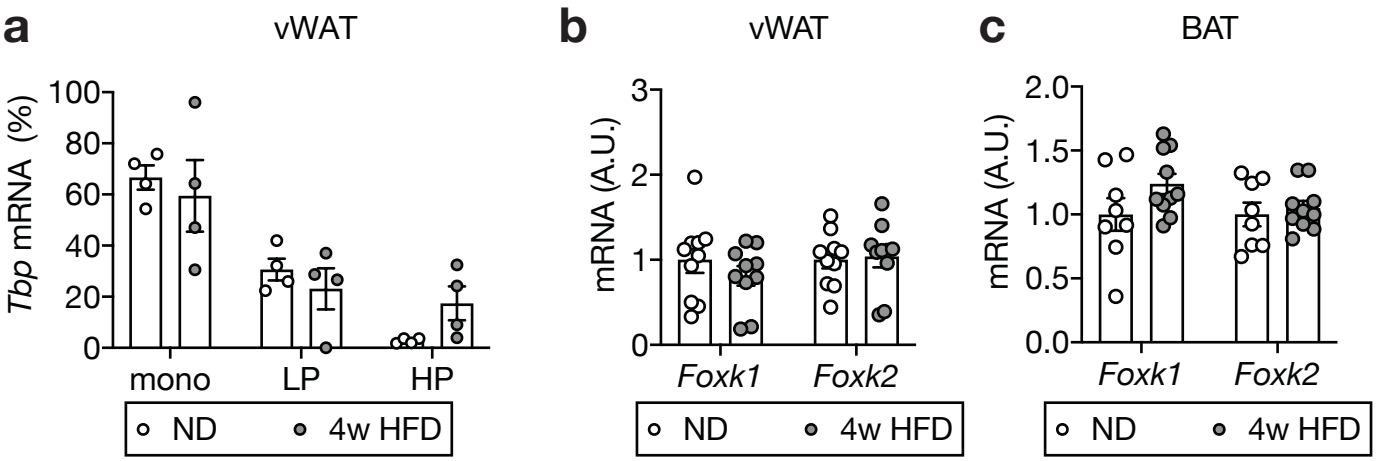

Extended Data Fig. 8. Mechanism of HFD-induced HK2 down-regulation in adipose tissue.
a. *Tbp* mRNA abundance in monosome (mono), light polysome (LP), and heavy polysome (HP) fractions in Fig. 4c. No significant difference in two-way ANOVA. n=4.
b. *Foxk1* and *Foxk2* mRNA levels in vWAT of ND- or 4-week HFD-fed wild-type C57BL6JRj mice. No significant difference in multiple t test. n=10 (ND) and 10 (HFD).
c. *Foxk1* and *Foxk2* mRNA levels in BAT of ND- or 4-week HFD-fed wild-type C57BL6JRj mice. No significant difference in multiple t test. n=8 (ND) and 10 (HFD).